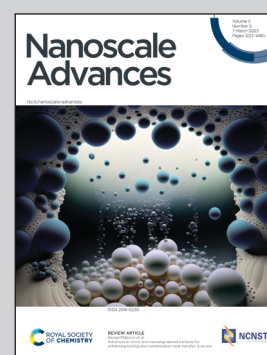


**Showcasing Nano-Ayur-Biology Research from Drug Discovery and Development Division, Patanjali Research Institute, Haridwar, Uttarakhand, India.**

*Withania somnifera*-derived carbon dots protect human epidermal cells against UVB-induced cell death and support growth factor-mediated wound healing

Carbon dot nanoparticles synthesized from *Withania somnifera* (L.) Dunal root extract and urea (*ws*CDs), using a one-step microwave method were found to protect human epidermal skin (A431) cells against UV induced damages. These  $14.4 \pm 0.18$  nm photoluminescent *ws*CDs were found to be biocompatible and to contain important phytochemicals derived from the plant. These *ws*CDs protected A431 cells from UV-induced oxidative damage by serving as antioxidant agents; and expedited wound healing by enhancing gene expression of growth-factors. Lastly, the *ws*CDs were also found to be enzymatically biodegradable through peroxidase-based biochemical reaction.



**As featured in:**



See Kunal Bhattacharya, Anurag Varshney *et al.*, *Nanoscale Adv.*, 2023, 5, 1331.

Cite this: *Nanoscale Adv.*, 2023, 5, 1331

# *Withania somnifera*-derived carbon dots protect human epidermal cells against UVB-induced cell death and support growth factor-mediated wound healing†

Acharya Balkrishna,<sup>abc</sup> Meenu Tomar,<sup>a</sup> Kunal Bhattacharya <sup>\*,a</sup>  
and Anurag Varshney <sup>\*,abd</sup>

Solar radiation comprising UVA and UVB regions is considered a skin-damaging factor inducing inflammation, oxidative stress, hyperpigmentation, and photo-aging. Photoluminescent carbon dots (CDs) were synthesized from the root extract of a *Withania somnifera* (L.) Dunal plant and urea, using a one-step microwave method. These *Withania somnifera* CDs (*wsCDs*) were  $14.4 \pm 0.18$  nm in diameter and presented photoluminescence. UV absorbance showed the presence of  $\pi-\pi^*$  (C=C) and  $n-\pi^*$  (C=O) transition regions in *wsCDs*. FTIR analysis indicated the presence of nitrogen and carboxylic functional groups on the surface of *wsCDs*. HPLC analysis of *wsCDs* showed the presence of withanoside IV, withanoside V, and withanolide A. The *wsCDs* were found to be biocompatible in human skin epidermal (A431) cells and hindered UVB irradiation-induced loss of metabolic activity and oxidative stress. The *wsCDs* supported rapid dermal wound healing through augmented TGF- $\beta$ 1 and EGF gene expression levels in A431 cells. Finally, *wsCDs* were found to be biodegradable through a myeloperoxidase-catalyzed peroxidation reaction. The study concluded that under *in vitro* conditions, *Withania somnifera* root extract-derived biocompatible carbon dots provided photo-protection against UVB-stimulated epidermal cell damage and supported rapid wound healing.

Received 16th August 2022  
Accepted 27th November 2022

DOI: 10.1039/d2na00545j

rsc.li/nanoscale-advances

## 1. Introduction

Sunlight is composed of 50% infrared, 40% visible, and 10% ultraviolet (UV) radiation. During outdoor activities, the skin is exposed to high levels of UV radiation depending upon the location on Earth, seasonal variation, and ozone layer thickness. Wavelengths of the solar UV radiation reaching the Earth's surface range between 290 and 400 nm and are further divided into UVA (400–315 nm) and UVB (315–290 nm) bands, which are typically present in a ratio of 41 : 1.<sup>1</sup> While UV exposure is beneficial for vitamin D production, too much of it can cause skin hyperpigmentation, photo-aging, cancer as well as sunburns that manifest as redness and painful blisters.<sup>2</sup> In order to reduce dangerous UV exposure during prolonged

outdoor activities, UV protection is administered in the form of sunscreen creams and sprays.

In recent times, the cosmetic industry has flooded the market with sunscreens featuring a variety of organic and inorganic active components. However, according to the Environmental Protection Group (EWG), only one of four products exhibits efficient UVA and UVB protection.<sup>3</sup> Additionally, a number of these sunscreens contain harmful chemicals that can injure individuals and the environment following an extended period of exposure. The United States Food and Drug Administration (US-FDA) has designated titanium dioxide (TiO<sub>2</sub>) and zinc oxide (ZnO) as GRASE ingredients up to a maximum level of 25 percent in certain over-the-counter sunscreen products.<sup>4</sup> Other studies, however, have raised concerns regarding the consequences of human exposure/co-exposure to both TiO<sub>2</sub> and ZnO nanoparticles that have been earlier reported as cyto and genotoxic.<sup>5,6</sup> In China, co-exposure of cosmetic shop assistants/clerks to TiO<sub>2</sub> and ZnO nanoparticles was found to elevate the levels of 8-hydroxy-2'-deoxyguanosine and creatinine in urine.<sup>7</sup>

Additionally, the non-biodegradable nature of inorganic sunscreens may make them accumulate and contribute to contamination of marine beaches, water, and aquatic life.

<sup>a</sup>Drug Discovery and Development Division, Patanjali Research Institute, Haridwar, India. E-mail: anurag@patanjali.res.in; anurag@prft.co.in; kunalbhattacharya@patanjali.res.in; kunalbhattacharya@prft.co.in

<sup>b</sup>Department of Allied and Applied Sciences, University of Patanjali, Haridwar, India

<sup>c</sup>Patanjali Yog Peeth (UK) Trust, 40 Lambhill Street, Kinning Park, UK

<sup>d</sup>Special Centre for Systems Medicine, Jawahar Lal Nehru University, New Delhi, India

† Electronic supplementary information (ESI) available. See DOI: <https://doi.org/10.1039/d2na00545j>



Research conducted in aquatic environments has shown that exposure to nanoforms of TiO<sub>2</sub> and ZnO may cause severe oxidative stress, and associated DNA strand breaks and adduct formations in organisms.<sup>8–10</sup> TiO<sub>2</sub> nanoparticle bioaccumulation in *Danio rerio* has been linked to altered hepatic superoxide dismutase levels, vacuolization, and disruption of the apical cytoplasm of intestinal epithelial cells.<sup>11</sup> Environmental risks have also been linked to organic UV filters and their photocatalytic derivatives, including benzophenone and butyl methoxydibenzoylmethane.<sup>12–14</sup> Hawaii has outlawed the use of sunscreens containing oxybenzone and octinoxate considering their contribution to marine pollution.<sup>15</sup> Hence, the priority of the cosmetic industry has now shifted toward the creation of environmentally benign nanomaterials, that can serve as broad-spectrum UV protectors and nanocosmeceuticals.

Zero-dimension organic nanoparticles called carbon dots (CDs) exhibit exceptional biocompatibility and possess special features such as high quantum yield, photostability, hydrophilicity, and functional tunability.<sup>16,17</sup> CDs have a diameter of less than 10 nm and are made up of carbon, hydrogen, nitrogen, and oxygen elements. Based on their chemical structure and surface functional groups, CDs can absorb a wide range of UV-irradiation and transform them into brilliant, tunable photoluminescence (PL).<sup>16,18</sup> Parallel to this, CDs can function as nanocosmeceuticals and drug carriers for targeted therapeutic approaches and are biodegradable reducing their environmental footprint and organ-based bioaccumulation.<sup>19,20</sup>

The Indian traditional medical system known as 'Ayurveda' uses herbal, herbo-mineral, and mineral-based formulations for preventive and therapeutic approaches against diseases. *Withania somnifera* (L.) Dunal (family: *Solanaceae*) (WS) also known as 'Winter Cherry' is a small woody plant growing in the Indian subcontinent region. The plant's common name is 'Aśvagandhā' (in Sanskrit). WS is considered a powerful plant showing excellent medicinal properties based on its phytochemical constituent triterpenoid steroidal lactones known as 'withanolides'.<sup>21</sup> Numerous studies have highlighted the anti-inflammatory, anti-tumor, cardioprotective, neuroprotective, and anti-microbial effects of withanolides.<sup>21–24</sup>

In this study, we used a one-step microwave-based synthesis technique to create CDs from WS root hydromethanolic extract (WS extract). We have used the dynamic light scattering method (DLS), UV spectroscopy, and Fourier transform infrared (FTIR) spectroscopy for examining the size distribution, zeta potential, chemical structure, and surface functional groups of WS CDs (*ws*CDs). We have used UV and fluorescence scans to further analyze the *ws*CDs' PL and UV absorption characteristics. We have scrutinized the biocompatibility, UVB protection, and anti-oxidant properties of *ws*CDs along with their growth factor-augmented wound healing qualities in human epidermal A431 cells. Finally, we investigated the oxidation-based enzymatic breakdown of *ws*CDs using a myeloperoxidase-based enzymatic degradation system to showcase their biodegradability and the stability of phytochemicals under different pH conditions.

## 2. Materials and methods

### 2.1 Reagents

The WS root sample was obtained from the herbal garden of the Patanjali Research Institute, Haridwar, India, and authenticated as per the Raw Materials Herbarium and Museum, CSIR-National Institute of Science Communication and Information Resources, Government of India, New Delhi, India (Authentication Voucher No. – NISCAIR/RHMD/Consult/2019/3453-54-15). The HPLC grade solvents acetonitrile, methanol, and orthophosphoric acid were obtained from Rankem, Gurugram, Haryana, India. Analytical grade potassium dihydrogen phosphate was procured from Merck & Co, Rahway, NJ, USA. Deionized water was obtained from a Milli-Q system (Millipore, Burlington, MA, USA). Standards for withanoside IV (purity, 96.2%), withanoside V (purity, 97.6%), withaferine A (Purity, 98.0%), withanolide A (purity, 97.5%), withanone (purity, 93.7%) and withanolide B (purity, 95.0%) were purchased from Natural Remedies, Bangalore, Karnataka, India.

### 2.2 Hydromethanolic extraction of the WS root by the reflux extraction method

Two kilograms of WS root powder was transferred into a round bottom flask and suspended in 10 L of hydromethanolic (water : methanol (1 : 1 v/v)) solvent. Solubilized phytochemicals were extracted in the hydromethanolic solvent at 65–70 °C for 2 h under reflux conditions with constant stirring. The extract was filtered through a 1 μm Whatman nitrocellulose filter paper and refluxed again under the same conditions. The filtrate was pooled and dried using a rota-evaporator at 40–50 °C under vacuum conditions. A light brown to brown colored powder was obtained with a yield of 10.8% w/w.

### 2.3 Preparation of *ws*CDs

Synthesis of *ws*CDs was performed by mixing 1.0 g of dry WS root extract powder and 1.0 g of urea in a 1:1 ratio. Four hundred μL of *N,N*-dimethylformamide solution was added to the mixture. The mixture was kept 2 cm away from the center in a 900 watts domestic microwave (LG Electronics, Seoul, South Korea; Model: MC2846SL), and irradiated at full power for 2 min. The charred mixture turned dark chocolate brown color and was then cooled to room temperature (RT). Fifty milliliters of MilliQ water was added to the charred mixture and the suspension was homogenized at 10 000 rpm for 10 min (Wiggen GmbH, Straubenhardt, Germany; Model: D-500). The homogenized solution was centrifuged at 13 000 rpm for 45 min to remove the larger particles, agglomerates, and residues. The supernatant was collected and dialyzed through a DiaEasy™ Dialyzer (20 ml) MWCO 1 kDa (BioVision Inc., Waltham, MA, USA) overnight in MilliQ water at RT under constant stirring at 100 rpm using a magnetic stirrer. The dialyzed sample was removed and hot air oven-dried at 50 °C. Dried *ws*CD samples were stored at 4 °C for long-term storage.



## 2.4 Determination of phytochemical content of *w*sCDs

Standards for withanoside IV, withanoside V, withaferine A, withanolide A, withanone, and withanolide B were dissolved in methanol individually to prepare 1000 ppm standard stock solutions. For the analysis, 50 ppm of standard mix working solution was prepared from each withanolide standard stock solution. *w*sCD and WS extract samples were suspended in MilliQ H<sub>2</sub>O at a 100 mg ml<sup>-1</sup> concentration for phytochemical profiling and processed for HPLC analysis. For pH stability of phytochemical analysis, 100 mg of *w*sCDs was suspended in 1 ml of MilliQ H<sub>2</sub>O with pH adjusted to 2.0, 7.0, and 10.0 and water-bath sonicated for 10 min in ice-cold H<sub>2</sub>O. The *w*sCD suspension was then incubated for 24 h at 37 °C. At the end of incubation, the particle suspension was filtered through a 0.1 μm PTFE syringe filter Whatman™ (Maidstone, United Kingdom). The filtrate was provided for HPLC analysis. HPLC-PDA analysis was performed on an HPLC (Prominence-iLC-2030c 3D Plus, Shimadzu, Japan) and separation was achieved using a Shodex C18-4E (5 μm, 4.6 × 250 mm) column subjected to binary gradient elution. A gradient solvent system of solvent A (prepared by dissolving 0.14 g potassium dihydrogen phosphate in 900 ml of water with the addition of 0.5 ml orthophosphoric acid and then diluting to 1000 ml with water) and solvent B (acetonitrile) was used. The gradient elution program used during the analysis consisted of 5–45% B for 0–18 min, 45–80% B from 18–25 min, 80% B from 25–28 min, 80–5% B from 28–30 min, and 5% B from 30–40 min. The flow rate was set at 1.5 ml min<sup>-1</sup> for chromatographic separation. The chromatographic detection of all the analytes was performed using a PDA detector at 227 nm. Temperature of the column was kept at 27 °C and the sample injection volume was 20 μl.

## 2.5 Particle size distribution and functional group analysis of *w*sCDs

For the analysis, 100 μg ml<sup>-1</sup> of *w*sCDs and WS extract were suspended individually in MilliQ H<sub>2</sub>O. The suspensions were mixed thoroughly using a bath-sonicator filled with ice-cold H<sub>2</sub>O for 15 min. Particle size distribution and zeta potential analysis were performed using a Malvern Zetasizer Advance Series (Malvern, UK) and analyzed using associated software. Fluorescence spectrum (300–750 nm) scans in varying UVB ranges (280–320 nm) and UV absorption scan (200–400 nm) of *w*sCDs and WS extract were performed using an Envision instrument (PerkinElmer, Waltham, MO, USA). Surface functional group analysis of the dry WS extract and *w*sCD samples was performed using a Cary 630 FTIR instrument (Agilent Scientific Instruments, Santa Clara, CA, USA). The acquired spectra were processed using Spectraglyph software (Software-Entwicklung, Oberstdorf, Germany).

## 2.6 A431 cell culture

Human epidermal A431 cells were obtained from the National Centre for Cell Science (NCCS), Pune (an Indian cell line repository for the American Type Culture Collection). The cells were grown in high-glucose DMEM-supplemented with 10% heat-inactivated FBS, 10 mM HEPES buffer, 100 IU ml<sup>-1</sup>

penicillin, 100 μg ml<sup>-1</sup> streptomycin and 1% non-essential amino acids. For determining the % metabolic activity and reactive oxygen species (ROS) studies, A431 cells were plated at a concentration of 1 × 10<sup>4</sup> per well in 96 well plates. For the cytotoxicity and gene expression studies, A431 cells were seeded at a density of 1 × 10<sup>5</sup> per well in 12 wells plates. The cells were pre-incubated overnight before the treatments.

## 2.7 Percentage metabolic activity and cytotoxicity analysis

For the dose–response study, A431 cells were treated with varying concentrations of *w*sCDs and WS extract for 24 h and % metabolic activity was measured using Alamar blue™ dye and in a separate set of experiments with Trypan blue® dye. Media alone was used as a negative control. For the UV irradiation study, the distance of the UV source from the bottom of the cell culture plate and treatment time were calibrated to 10 cm distance for 30 min exposure. A431 cells were pre-treated with varying *w*sCD and WS extract concentrations and incubated for 24 h. For UVB irradiation, the treatment medium containing *w*sCDs was removed from the A431 cells. Cells were washed with sterile phosphate-buffered saline (PBS) solution and 100 μl of PBS was added to each well. A431 cells were then irradiated with UVB for 30 min at a 10 cm distance from the light source. PBS was then again replaced with the respective treatment medium containing *w*sCDs and further incubated for 24 h. On the next day, % metabolic activity was measured using the Alamar blue™ assay and cytotoxicity was measured using Trypan blue® dyes. Fluorescence spectra of the metabolized Alamar blue™ was measured at ex. 560 nm/em. 580 nm wavelengths using an EnVision multimode plate reader (PerkinElmer, Waltham, MA). Cell metabolic activity percentages under all the conditions were calculated for treated *versus* unexposed controls. For the cytotoxicity study, Trypan blue® treated A431 cells were measured for the number of viable *versus* dead cells using a Biorad TC20 automated cell counter (Hercules, CA, USA).

## 2.8 Intracellular ROS determination

A431 cells were pre-treated with varying *w*sCD concentrations and incubated for 24 h. For UVB irradiation, the treatment medium containing *w*sCD was removed from the A431 cells. Cells were washed and soaked in 100 μl of PBS in each well. A431 cells were then irradiated with UVB for 30 min at a 10 cm distance. PBS was then again replaced with the respective treatment medium containing *w*sCDs and further incubated for 2 h and 24 h. At the end of the treatment time, cells were washed with sterile PBS and treated with 2',7'- dichlorofluorescein diacetate dye (10 μg ml<sup>-1</sup>) mixed in serum-free culture media. Cells were incubated in the dark for 45 min at 37 °C and then washed with PBS to remove the extracellular dye. The fluorescence intensity of the transformed dichlorofluorescein dye was measured using the ex: 490 nm/em: 520 nm wavelengths using an EnVision multimode plate reader (PerkinElmer, Waltham, MA).

## 2.9 Gene expression study

A431 cells were pre-treated with varying *w*sCD concentrations and incubated for 24 h and then treated with UVB as mentioned



previously. At 24 h post-UVB irradiation and *ws*CD therapeutic treatment, A431 cells were washed with cold PBS and lysed using RNeasy lysis buffer (Qiagen, Frederick, MD) liberating the total RNA content. Complementary DNA (cDNA) was synthesized using a one-step Verso cDNA synthesis kit (ThermoFischer Scientific Inc., Waltham, MA). The primers used in the study were:

Transforming growth factor-beta 1 (TGF- $\beta$ 1; NCBI Gene ID: 7040): FW: 5'CAATTCCTGGCGATACCTCAG3', REV: 5'GCACAACTCCGGTGACATCAA3'.

Epidermal growth factor (EGF; NCBI Gene ID: 1950): FW: 5'GTGCAGCTTCAGGACCACAA3', REV: 5'AAATGCATGTGTCGAATATCTTGAG3'.

Beta-actin ( $\beta$ -actin; house-keeping gene: NCBI Gene ID: 11461): FW: 5'GGCTGTATTCCCTCCATCG3', REV: 5'CCAGTTGTAACAATGCCATGT3'.

All the primers were mixed with SYBR-green universal master mix and real-time PCR (RT-PCR) assay was run on a qTower3G RT-PCR instrument (Analytik-Jena AG, Jena, Germany). Conditions were set as 40 cycles per RT-PCR run with denaturation at 95 °C for 10 min, annealing at 60 °C for 1 min, and extension at 75 °C for 15 s. Based on the obtained ' $C_t$  values', relative mRNA expression fold changes were calculated.

## 2.10 Wound healing (scratch assay)

For the assay,  $1 \times 10^5$  A431 cells were plated in 12 well plates and pre-incubated overnight. The next day, cells were pre-treated with varying concentrations of *ws*CDs and incubated for 24 h. For the scratch assay, the old treatment medium of the cells was removed from the cells and 1 ml of sterile PBS was added to each well. Scratch was introduced using a sterilized

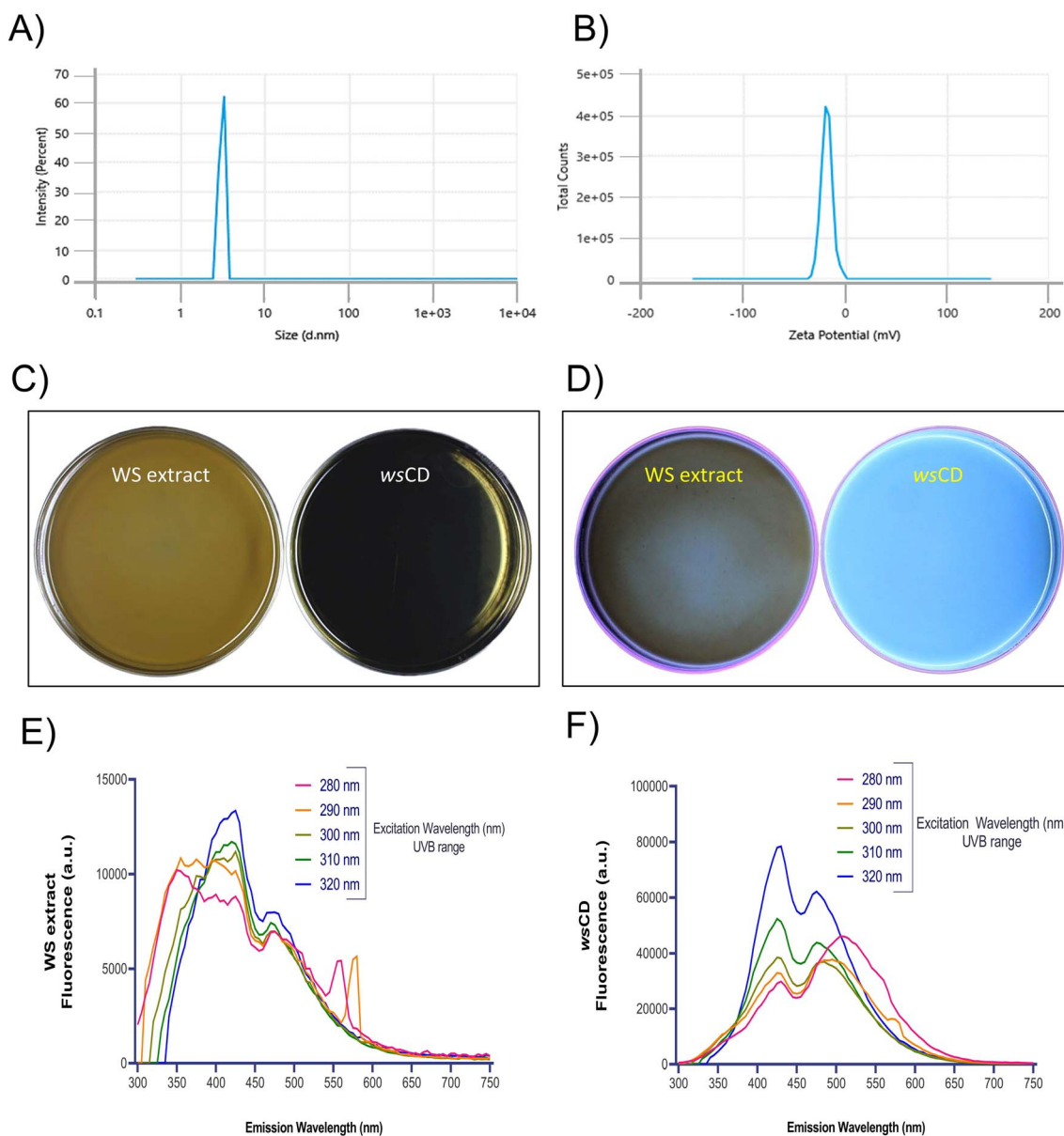


**Fig. 1** Physicochemical analysis of *ws*CDs and WS extract. (A) Particle size distribution of carbon dots; (B) zeta potential of carbon dots; (C) image of WS extract and *ws*CDs under white light; (D) photoluminescence of WS extract and *ws*CDs under UV excitation; (E) fluorescence emission scan of WS extract at varying UVB excitation wavelengths; (F) fluorescence emission scan of *ws*CDs at varying UVB excitation wavelengths.



200  $\mu\text{l}$  pipette tip and then washed with PBS for removing the detached cells. Fresh media containing varying  $\omega\text{sCD}$  concentrations were given to their respective wells and images were acquired for each well through a marked region (single location per well) between 0 and 10 h at 2 h intervals, using a Zeiss Promovert (Zeiss AM, Oberkochen, Germany) inverted microscope attached to Zeiss AxioVision software (version 4.9.1.0). Images were analyzed using ImageJ software using the macro 'wound healing size tool'.<sup>25,26</sup> The parameters selected for the analysis were wound width ( $\mu\text{m}$ ) and wound healing percentage calculated using the imageJ software using the eqn (1) (ref. 26)

$$\text{Wound healing (\%)} = (A(t_0) - A(t_\Delta)) / (A(t_0)) \quad (1)$$

where ' $A(t_0)$ ' is the initial wound area and ' $A(t_\Delta)$ ' is the wound area after ' $n$ ' hours of the initial scratch, both measurements were calculated in ' $\mu\text{m}^2$ '.

### 2.11 Enzymatic biodegradation study

Enzymatic degradation assay was performed following the protocol mentioned by Mukherjee *et al.*<sup>27</sup> Mixtures containing 5

$\mu\text{g ml}^{-1}$  human origin MPO (Merck, Rahway, NJ, USA) per 50  $\mu\text{g}$  of  $\omega\text{sCDs}$  (final concentration 100  $\mu\text{g ml}^{-1}$ ) were suspended in 1 ml of autoclaved Milli-Q water containing 140 mM NaCl.  $\text{H}_2\text{O}_2$  was added at a rate of 100  $\mu\text{M h}^{-1}$  for 24 h. The MPO enzyme was replenished after 6 h and the reaction mixture was maintained at 37  $^\circ\text{C}$ . Equal amounts of  $\omega\text{sCDs}$  were suspended in 1 ml of autoclaved Milli-Q  $\text{H}_2\text{O}$  and treated with/without  $\text{H}_2\text{O}_2$  added at a rate of 100  $\mu\text{M h}^{-1}$  for 24 h. At the end of the reaction time, the samples were immediately analyzed using a UV-1800 spectrometer (Shimadzu, Kyoto, Japan) for absorbance between 300 and 500 nm. The acquired spectra were processed using Spectraglyph software.

### 2.12 Statistical analysis

All the experiments were performed in technical and biological triplicate and the results were presented as the mean  $\pm$  SD. The results were analyzed by one-way ANOVA followed by Tukey's *post hoc* test using Graphpad software (GraphPad Software, Inc., La Jolla, CA, USA). Differences were considered statistically significant if  $p$ -value  $<$  0.05.

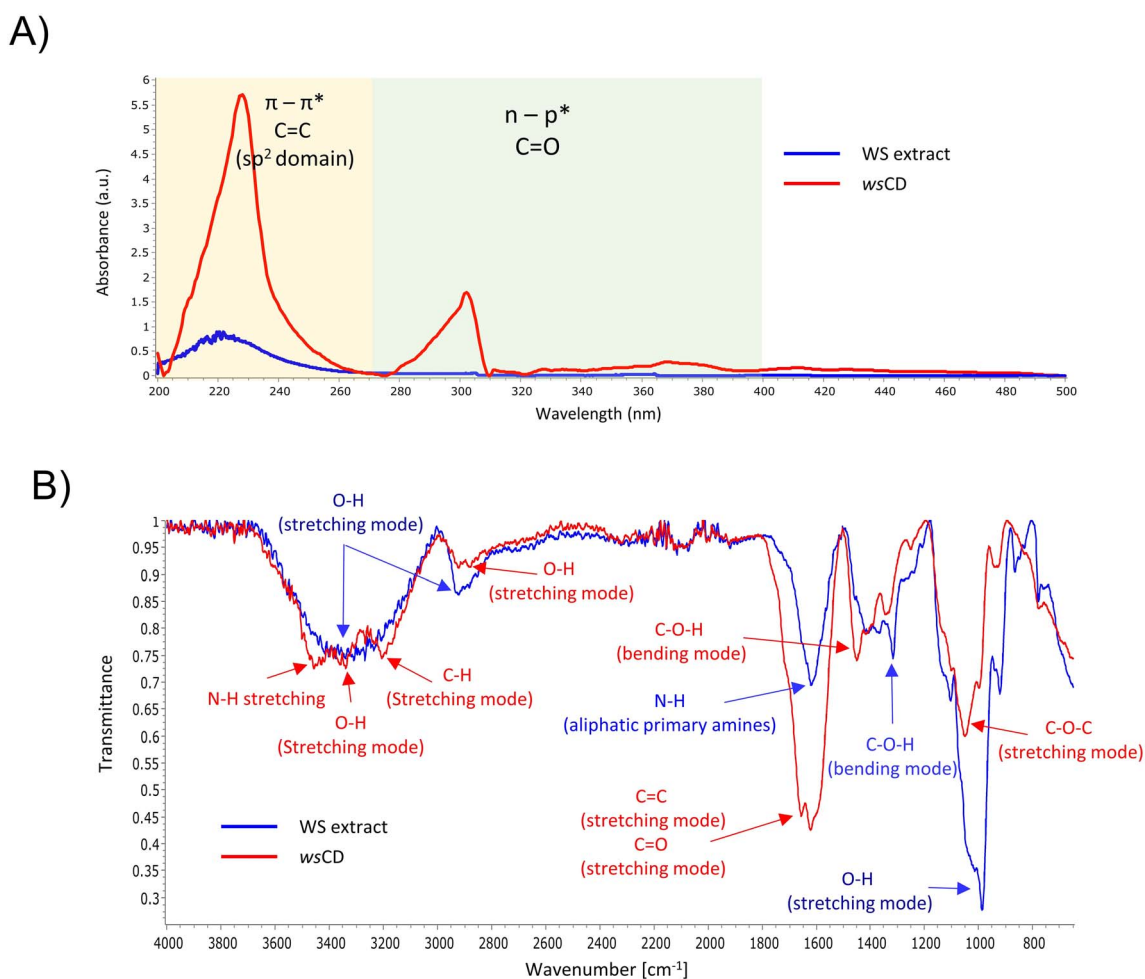


Fig. 2 Chemical structure and surface functional group analysis. (A) Chemical structure analysis of WS extract and  $\omega\text{sCDs}$  using UV absorption spectroscopy; (B) surface functional group analysis of WS extract (blue) and  $\omega\text{sCDs}$  (red) using Fourier transform infrared spectroscopy.



**Table 1** HPLC-based phytochemical profiling of WS extract and wsCDs (representative HPLC spectra: Fig. 3A and B). ND = not detected

S. No.	Marker compounds	WS extract ( $\mu\text{g mg}^{-1}$ )	wsCD ( $\mu\text{g mg}^{-1}$ )
1	Withanoside IV	1.604	1.998
2	Withanoside V	0.779	1.168
3	Withaferine A	0.916	ND
4	Withanolide A	0.749	0.047
<b>Total withanolide</b>		<b>4.048</b>	<b>3.213</b>

### 3. Results and discussion

#### 3.1 Synthesis and physicochemical characterization of wsCDs

CDs can be fine-tuned in their functionality and PL properties through manipulation of their surface functional groups and chemical structures. In a recently published review, Ethordevic *et al.* put together a toolbox for the synthesis of CDs that may be functionalized according to their application needs.<sup>16</sup> CDs may be created either by a top-down approach through disassembling of large carbon structures or by a bottom-up approach by constructing them from smaller carbon precursors. In the latter case, CDs are created using combustion/thermal/microwave/solvothermal techniques. One-step microwave-based synthesis

of CDs has grown in popularity since it is an inexpensive method and produces little residual waste.<sup>28</sup>

A 900 watt domestic microwave was used to synthesize wsCDs from a 1 : 1 ratio (w/w) mixture of WS extract and urea. These wsCDs had a hydrodynamic diameter of  $14.4 \pm 0.18$  d nm (Fig. 1A) and a zeta potential of  $-3.9 \pm 2.7$  mV (Fig. 1B). In contrast, WS extract showed a size distribution of more than 1  $\mu\text{m}$  (data not shown). Urea serves as a nitrogen functional group donor in this synthesis, presenting N-H groups on the surface of wsCDs.<sup>16</sup> Contrasting with the turbid brown characteristic of their parent WS extract, the wsCDs projected a chocolate brown hue under ambient light (Fig. 1C). The synthesized wsCDs showed a blue colored PL when excited at UVB range wavelengths of 280–320 nm (Fig. 1D and F). In contrast, WS extract showed a low intensity fluorescence emission possibly originating from the presence of fluorescent aromatic and phenolic natural compounds (Fig. 1D and E).<sup>29</sup> Maximum PL emission from the wsCDs was found at ex. 320 nm with an em. at 430 nm (Fig. 1F). The intensity of PL from wsCDs was 6 $\times$  times higher than that of PL from WS extract at the highest emission wavelength (ex. 320 nm and ex. 430 nm) (Fig. 1E and F). In CDs, the presence of emissive traps, triplet carbenes at the zigzag edges, aromatic conjugate structures, and attached chemical groups such as carboxyl and oxygen-rich hydroxyl groups all contribute to the blue color PL.<sup>30–32</sup>

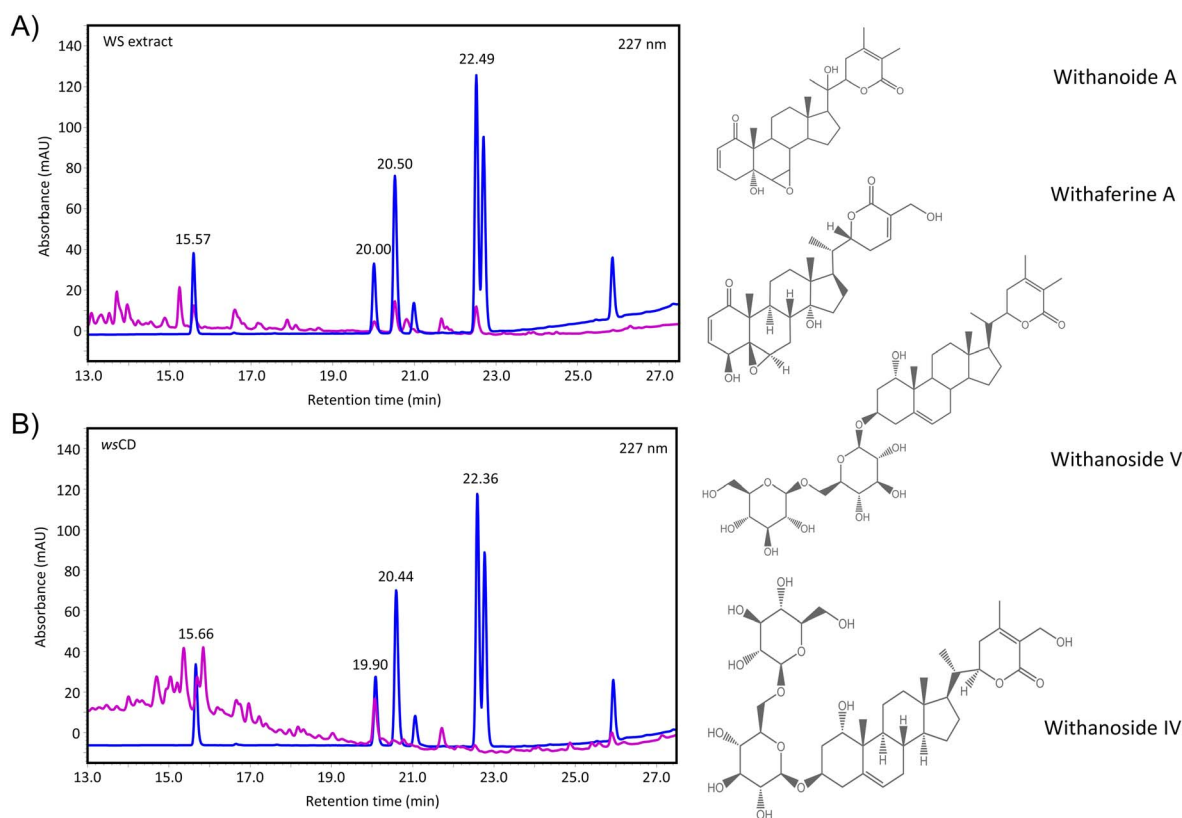


**Fig. 3** Phytochemical profiling of wsCDs and WS extract. (A) High-performance liquid chromatography analysis of WS extract for phytochemical profiling: withanoside IV (15.57 min); withanoside V (20.00 min); withaferine A (20.50 min), and withanolide A (22.49 min) (B) high-performance liquid chromatography analysis of wsCDs for phytochemical profiling: withanoside IV (15.66 min); withanoside V (19.90 min); withaferine A (20.44 min), and withanolide A (22.36 min). Quantitative data are presented in Table 1. The complete HPLC spectral range is provided in ESI Fig. S1A and B.†



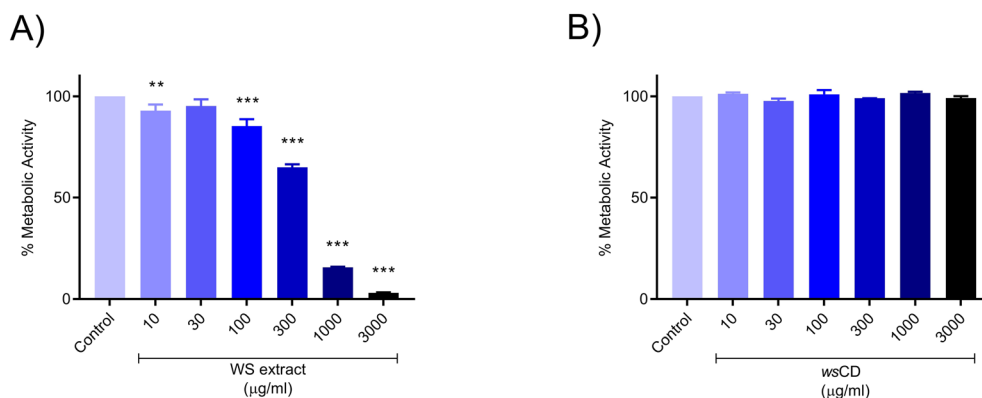


Fig. 4 Biocompatibility study, (A) dose–response of WS extract in A431 cells during 24 h of exposure; (B) dose–response of wsCDs in A431 cells during 24 h of exposure. The results represent mean  $\pm$  SD. Statistical analysis through one-way ANOVA followed by Tukey's *post hoc* test (control vs. varying doses). \*\**p*-value < 0.01; \*\*\**p*-value < 0.001.

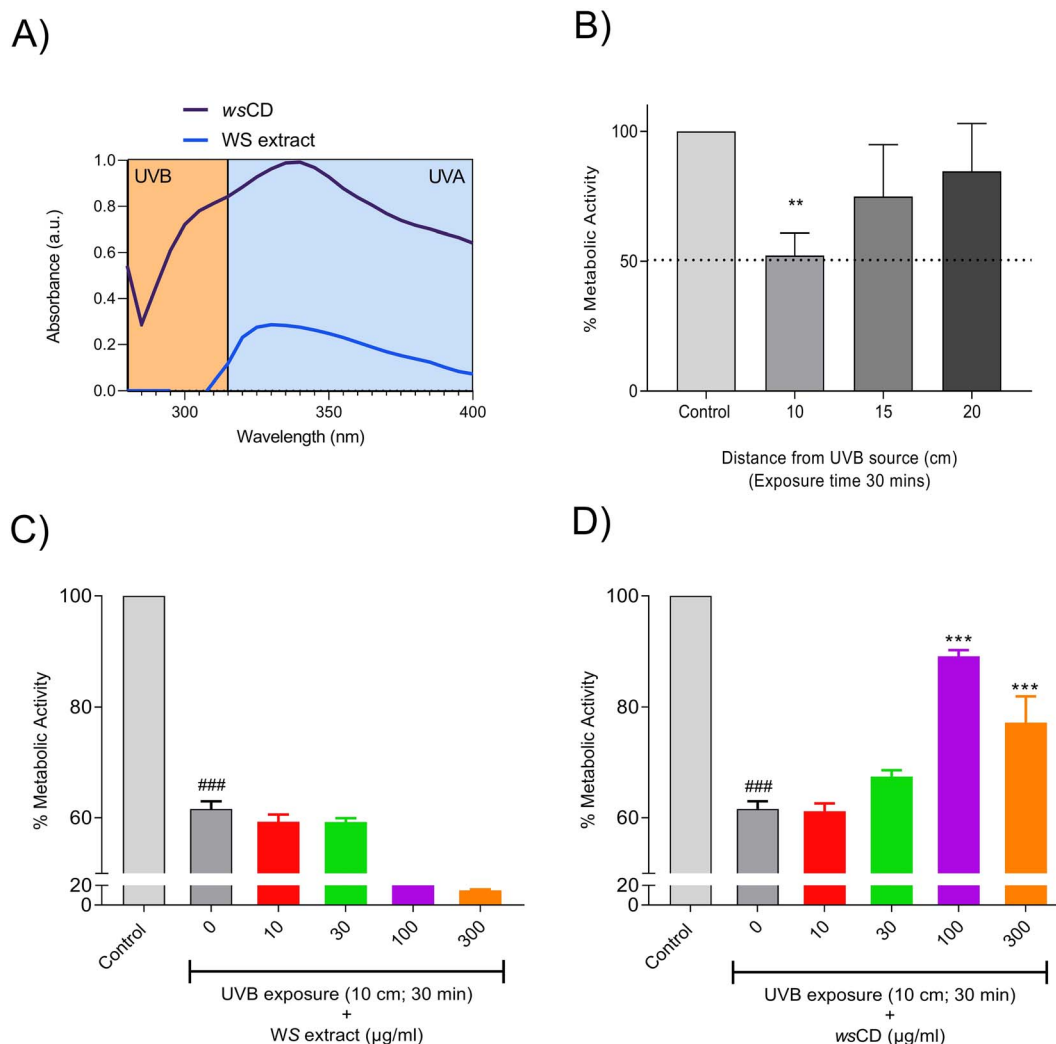


Fig. 5 UV protection activity of WS extract and wsCDs. (A) Comparative UVA and UVB regions' (200–400 nm) absorbance at a 100 μg ml concentration of wsCDs and WS extract; (B) calibration of UVB irradiation in A431 cells on the basis of cell viability loss at 30 min exposure time and 10, 15, and 20 cm distance between cells and the light source; (C) UVB photo-protection of WS extract at varying doses in A431 cells during 24 h of exposure; (D) UVB photo-protection of wsCDs at varying doses in A431 cells during 24 h of exposure. The results represent mean  $\pm$  SD. Statistical analysis through one-way ANOVA followed by Tukey's *post hoc* test. ###*p*-value < 0.001 (control vs. UVB treatment); \**p*-value < 0.05; \*\**p*-value < 0.01; \*\*\**p*-value < 0.001.





UV spectrum analysis of *ws*CDs revealed absorbance between 200 and 270 nm, with the  $\lambda_{\text{max}}$  at 227 nm (Fig. 2A). This region of the UV absorbance spectrum has been attributed to the  $\pi$ - $\pi^*$  transitions of C=C bonds belonging to the carbon core of the  $\text{sp}^2$  domain.<sup>33</sup> A second UV absorbance shoulder peak was observed between 279 and 400 nm range ascribed to the  $n$ - $\pi^*$  transition of C=O surface groups.<sup>33</sup> As a result, the chemical structure of *ws*CDs revealed the existence of  $\text{sp}^2$  transition C=C and C=O bonds (Fig. 2A). Other CDs synthesized from herbal and animal origin sources have shown a similar presence of  $\pi$ - $\pi^*$  and  $n$ - $\pi^*$  electronic transition regions in their UV absorbance spectra.<sup>34,35</sup> It is interesting to note that these previous investigations have also reported a brilliant blue PL emission from their CDs when exposed to UV light, which is comparable to that from *ws*CDs. FTIR spectroscopy reveals the chemical nature of functional groups present on the surface of the nanomaterials. FTIR analysis of the *ws*CDs revealed the presence of N-H and O-H (stretching modes) between 3463 and 3186  $\text{cm}^{-1}$ , C-H (stretching mode) at 2920  $\text{cm}^{-1}$ , large C=C (stretching mode) at 1662  $\text{cm}^{-1}$ , C=O (stretching mode) at 1600  $\text{cm}^{-1}$ , C-O-H (bending mode) at 1412  $\text{cm}^{-1}$ , and C-O-C

(stretching mode) at 1069  $\text{cm}^{-1}$  (Fig. 2B). Similar functional groups have been observed previously using FTIR in other synthesized CDs.<sup>36-39</sup> The results revealed the presence of amino and carboxylic groups on the surface of the *ws*CDs originating from the urea doping and microwave-based oxidation process. In the WS extract, O-H (stretching mode) was observed at 3308 and 2922  $\text{cm}^{-1}$  originating from compounds containing phenol and carboxylic acid (Fig. 2B). A peak originating from N-H originating from aliphatic primary amines was observed at 1618  $\text{cm}^{-1}$ . A peak originating from C-O-H was observed at 1316  $\text{cm}^{-1}$  originating from phenol (Fig. 2B). FTIR peaks originating from different phytochemicals present in the WS extract have been extensively discussed by Das *et al.*<sup>40</sup> HPLC analysis showed the presence of withanoside IV, withanoside V, and withanolide A phytochemicals in *ws*CDs (Table 1). Due to the loss of withaferin A in *ws*CDs, the overall withanolide concentration (3.21  $\mu\text{g mg}^{-1}$ ) was found to be lower than that of WS extract (4.05  $\mu\text{g mg}^{-1}$ ) (Fig. 3A and B; Table 1 and ESI Fig. S1A and B†). Studies using the microwave process have shown that withaferin A is liberated from WS extract.<sup>41</sup> Hence, it is possible that the microwave-based synthesis process and dialysis of the

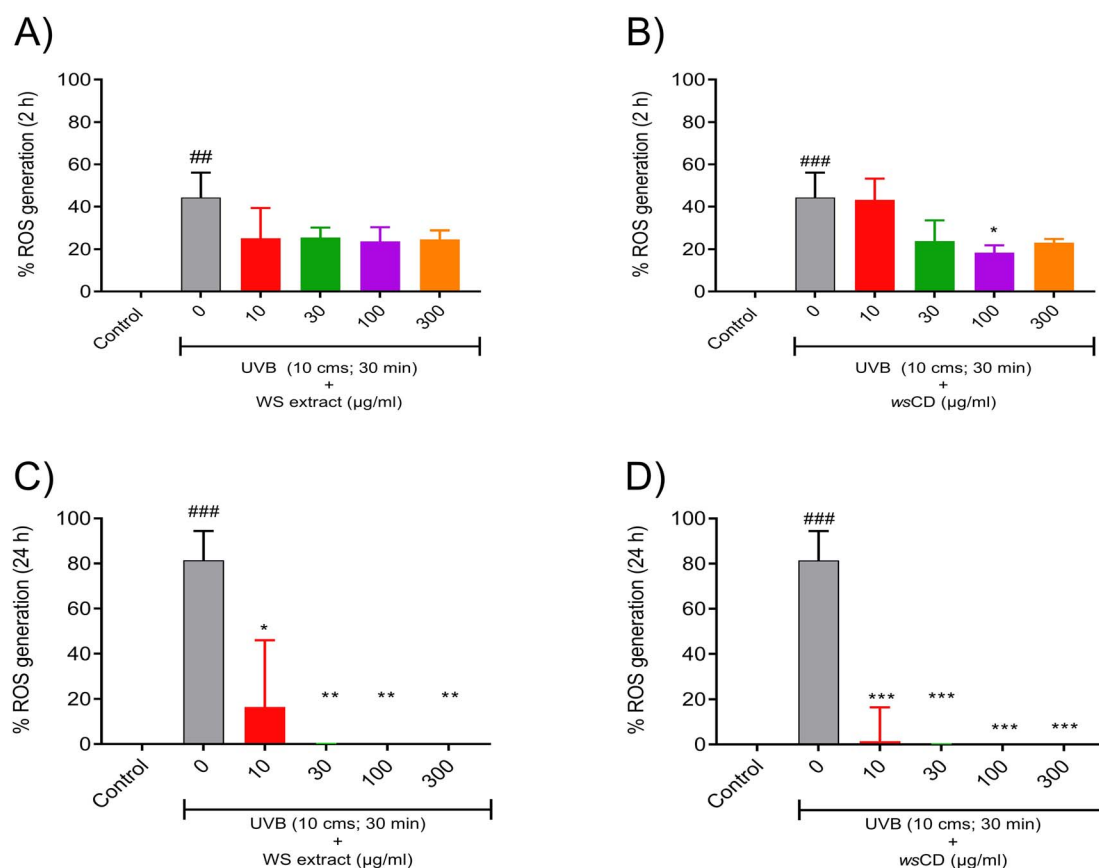


Fig. 6 Antioxidant activities of WS extract and *ws*CDs. (A) Antioxidant activity of WS extract in A431 cells 2 h post-UVB irradiation; (B) antioxidant activity of *ws*CDs in A431 cells 2 h post-UVB irradiation; (C) antioxidant activity of WS extract in A431 cells during 24 h post-UVB irradiation. (D) Antioxidant activity of *ws*CDs in A431 cells during 24 h post-UVB irradiation. The results represent mean  $\pm$  SD. Statistical analysis through one-way ANOVA followed by Tukey's *post hoc* test. ##  $p$ -value  $< 0.01$  (control vs. UVB treatment), ###  $p$ -value  $< 0.001$  (control vs. UVB treatment); \*  $p$ -value  $< 0.05$ ; \*\*  $p$ -value  $< 0.01$ ; \*\*\*  $p$ -value  $< 0.001$ .



wsCDs might have completely removed withaferin A from nanoparticles (Table 1).

### 3.2 Biocompatibility, photo-protection, and antioxidant activity of wsCDs

Treatment of the A431 cells with WS extract showed a significant ( $p$ -value < 0.01) induction of cellular metabolic activity loss with a 50% inhibitory concentration determined at  $440.5 \mu\text{g ml}^{-1}$  (Fig. 4A). On the other hand, the wsCDs were found to be biocompatible in human epidermal (A431) cells up to the

measured dose of  $3000 \mu\text{g ml}^{-1}$  and an exposure period of 24 h using % cell metabolic activity (Alamar blue™) assay (Fig. 4B). No response was observed in the A431 cells based on Trypan blue following treatment with both the WS extract and wsCDs (data not shown). This could be due to the lack of Trypan blue® assay sensitivity in comparison to the Alamar blue™ assay.<sup>42</sup>

Due to their absorbance in the UVA (315–400 nm) and UVB (280–315 nm) regions, CDs and their composites have gained importance as UV protectors.<sup>18,43–46</sup> In comparison to their parent materials (WS extract), wsCDs showed a 3.6× enhanced

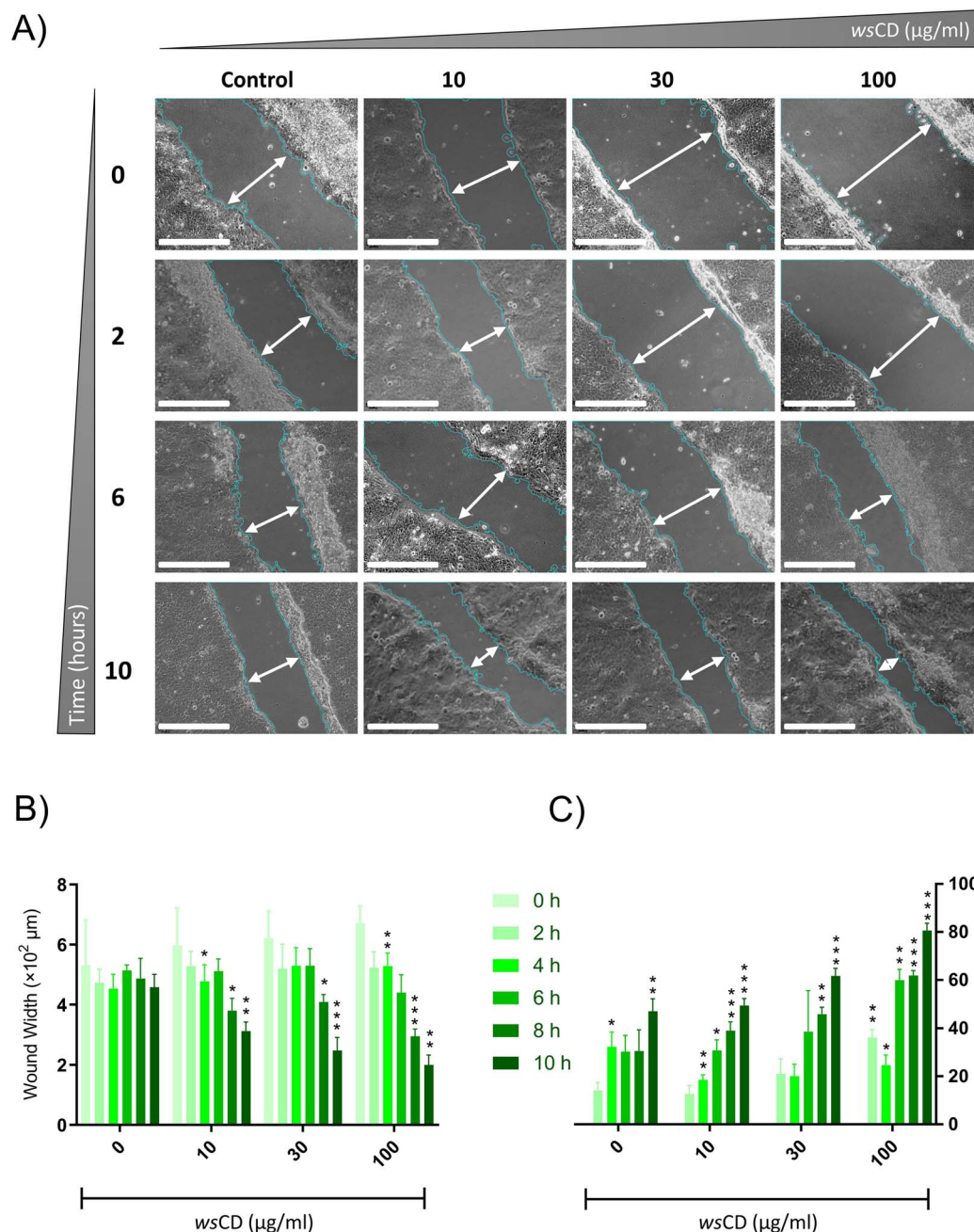


Fig. 7 Wound healing properties of wsCDs. (A) Scratch assay analysis of A431 cells treated with varying concentrations of wsCDs over a period of 10 h. Microscopy images were acquired for analysis every 2 h (scale bar – 200  $\mu\text{m}$ ); (B) scratch wound width ( $\mu\text{m}$ ); (C) scratch wound healing percent. The results represent mean  $\pm$  SD. Statistical analysis through one-way ANOVA followed by Tukey's *post hoc* test. \* $p$ -value < 0.05; \*\* $p$ -value < 0.01; \*\*\* $p$ -value < 0.001 (0 h vs. treatment time).



absorbance ( $\lambda_{\max}$  – 340 nm) in the UV regions of 280–400 nm at an equal concentration of  $1 \text{ mg ml}^{-1}$  (Fig. 5A). For the *in vitro* UV protection assay, we used UVB (narrow-band 311 nm) as a cellular damage inducer in the cutaneous A431 cells. We measured the metabolic changes induced by UVB irradiation in the A431 cells after 30 min of exposure from a distance of 10, 15, and 20 cm using a 9 W UVB light source (Philips PL-S 9W/01/2P). We observed that at a distance of 10 cm UVB (narrow band 311 nm) caused a detrimental ( $p$ -value < 0.01) loss in cellular metabolic activity ( $52.19 \pm 8.61\%$ ) in A431 cells following 30 min of treatment time (Fig. 5B). Pre-treatment of the A431 cells with WS extract did not provide any photo-protection against UVB exposure (Fig. 5C). A significant ( $p$ -value < 0.001) photo-protective effect of *ws*CDs was observed at  $100 \mu\text{g ml}^{-1}$  ( $89.08 \pm 1.15\%$ ) and  $300 \mu\text{g ml}^{-1}$  ( $77.17 \pm 4.76\%$ ) against UVB-induced loss of metabolic activity after pre- and post-treatment in the A431 cells (Fig. 5D). Using CDs made from *Dunaliella salina* (microalgae) as a preventative therapy, Chatzimitakos *et al.* demonstrated photo-protection in human keratinocytes (HaCat cells) against UV irradiation (314 nm) at the tested concentrations of 100 and 200  $\mu\text{g ml}^{-1}$ .<sup>43</sup>

The formation of reactive oxygen species (ROS) by catalase activity under UVB irradiation has been shown to cause oxidative stress-based cellular damage.<sup>47</sup> In the present study, UVB treatment induced significant ( $p$ -value < 0.001) levels of intracellular ROS in A431 cells after 2 h and 24 h treatments (Fig. 6A–D). Pre- and post-treatment of UVB-exposed A431 cells with WS extract reduced the formation of intracellular ROS, showing that antioxidant action is possibly derived from the presence of phytochemicals (Fig. 6A and C). *ws*CD pre- and post-treatment also considerably ( $p$ -value < 0.001) reduced UVB-induced ROS levels in A431 cells at 2 h ( $44.34 \pm 11.76\%$ ) and 24 h ( $81.55 \pm 13.01\%$ ) post-irradiation (Fig. 6B and D). Beneficial phytochemicals such as withanoside V are known to have excellent free radical scavenging activity.<sup>48,49</sup> Withanolides (1-oxo-5- and 6-beta-epoxy-with-2-enolide) discovered in WS extract have been

shown to protect skin against UVB-induced malignancies through irradiation absorption and antioxidant activity.<sup>50</sup>

### 3.3 Growth factor assisted wound healing properties of *ws*CDs

While UV radiation protection from sun-protective chemicals and composites can last for a long time, they are unable to fully protect the skin from long-term UV exposure. Normal A431 cells were used in the scratch analysis experiment, which revealed that *ws*CD-treated cells showed a better wound healing response than control ( $0 \mu\text{g ml}^{-1}$  *ws*CD) cells (Fig. 7A). Substantial ( $p$ -value < 0.01) wound closure was observed on the basis of the wound width and wound healing percent in the A431 cells treated with a  $100 \mu\text{g ml}^{-1}$  concentration of *ws*CDs at a measured time period of 10 h (Fig. 7B and C). A combination of UVB treatment in scratched A431 cells led to unrecoverable damage that did not support wound healing (data not shown). Growth factors play a major role in cell proliferation and wound healing processes. Transforming growth factor beta-1 (TGF- $\beta$ 1) and epidermal growth factor (EGF) are two key growth factors that were screened in the current investigation. TGF- $\beta$ 1 participates in a variety of wound healing processes, including inflammation, angiogenesis stimulation, fibroblast proliferation, collagen synthesis, extracellular matrix (ECM) deposition, and remodeling.<sup>51</sup> EGF is also regarded as a crucial growth factor that contributes to the creation of granulation tissue, ECM component synthesis, keratinocyte migration, keratinocyte proliferation, and fibroblast activity during the healing of wounds.<sup>52</sup> In the present study, UVB treatment alone in A431 cells induced a  $1.53 \pm 0.37$ -fold increase in the TGF- $\beta$ 1 and a  $1.37 \pm 0.02$ -fold increase in the EGF mRNA expression levels compared to those in the unexposed cells (Fig. 8A and B). TGF- $\beta$ 1 mRNA expression levels further increased significantly ( $p$ -value < 0.001) in UVB-irradiated A431 cells treated with varying concentrations of *ws*CDs (Fig. 8A). EGF mRNA expression levels were also significantly ( $p$ -value < 0.05) elevated in UVB-irradiated A431 cells treated with  $100 \mu\text{g ml}^{-1}$  *ws*CD (Fig. 8B). Hence, *ws*CDs stimulated a high mRNA expression of

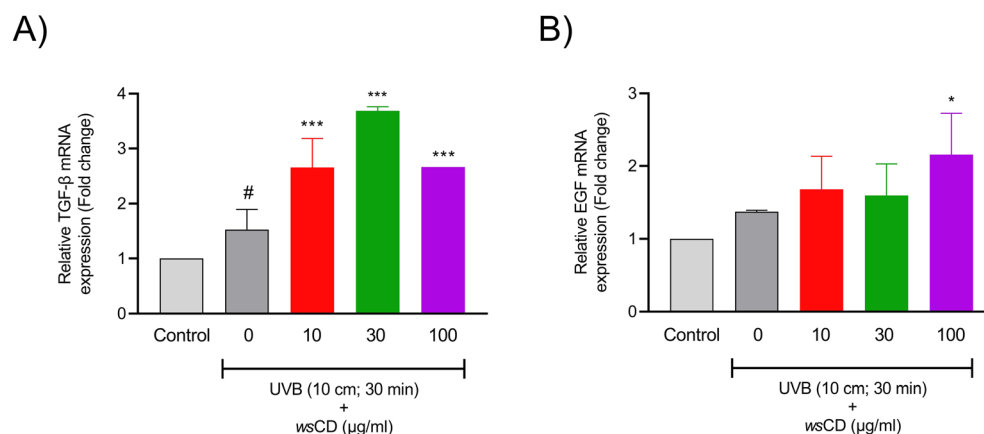


Fig. 8 Growth factor mRNA expression. (A) Transforming growth factor-beta 1 (TGF- $\beta$ 1) mRNA expression in UVB irradiated A431 cells pre- and post-treated with *ws*CDs. (B) Epithelial growth factor (EGF) mRNA expression in UVB irradiated A431 cells pre- and post-treated with *ws*CDs. The results represent mean  $\pm$  SD. Statistical analysis through one-way ANOVA followed by Tukey's *post hoc* test. # $p$ -value < 0.05 (control vs. UVB treatment); \* $p$ -value < 0.05; \*\*\* $p$ -value < 0.001.



the growth factors EGF and TGF- $\beta$ 1 that might be related to the enhanced wound repair observed in the scratch assay (Fig. 7 and 8). UVB triggers TGF- $\beta$ 1 and EGF signaling in irradiated keratinocytes through the production of ROS and G-protein  $\beta\gamma$  subunit signaling pathways, respectively.<sup>53-55</sup> Chronic and non-healing wounds often show a loss of TGF- $\beta$ 1 signaling.<sup>56</sup> While no study has reported the effect of WS extract on keratinocyte EGF mRNA expression levels, it has been found to promote TGF- $\beta$ 1 mRNA expression in HaCat cells.<sup>57</sup> Future studies would focus on intracellular delivery and release of individual phytochemicals loaded on wsCDs into epidermal cells and the role of these phytochemicals in stimulating rapid wound healing.

### 3.4 Enzymatic biodegradability of the wsCDs

Studying the wsCD biodegradability is crucial in addition to proving their biocompatibility, photo-protective and therapeutic qualities. Human myeloperoxidase and eosinophil peroxidase enzymes have been shown to enzymatically break-down the graphitic structure of CDs and other carbonaceous nanomaterials through the oxidation reaction.<sup>20,58</sup> Hence, we investigated the oxidative biodegradation of wsCDs using an MPO-based peroxide system. UV spectroscopy analysis of wsCDs showed a reduction in the n-p\* transition region (C=O) absorbance after 24 h of incubation with 5  $\mu\text{g ml}^{-1}$  MPO, 140 mM NaCl, and 100  $\mu\text{M H}_2\text{O}_2$  compared to the wsCDs suspended in  $\text{H}_2\text{O}$  (Fig. 9A and B).  $\text{H}_2\text{O}_2$  alone also caused oxidative degradation of the wsCDs which was less compared to that caused by the MPO, NaCl, and  $\text{H}_2\text{O}_2$ -driven peroxide system

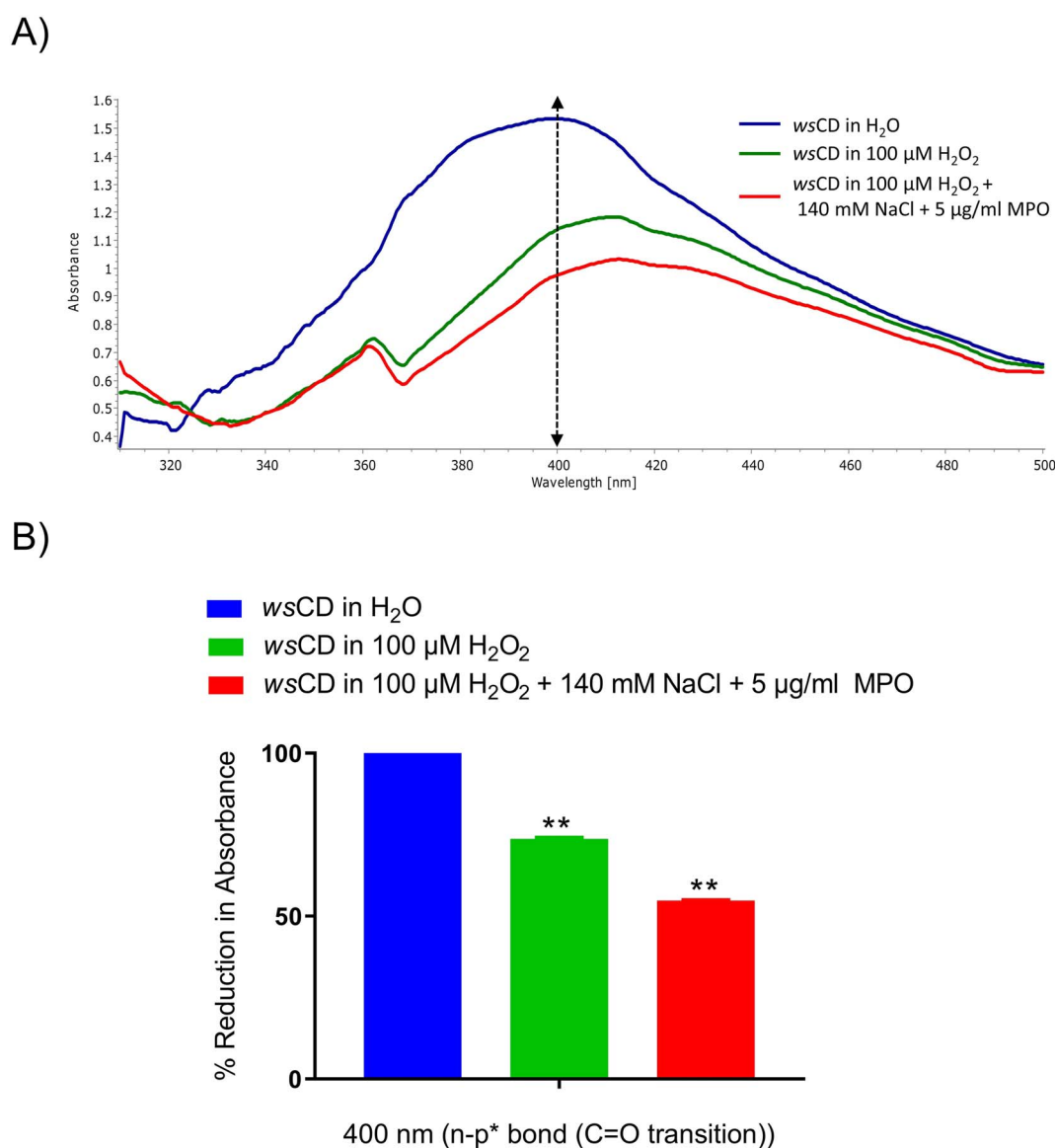


**Fig. 9** Enzymatic biodegradation of wsCDs. (A) UVB absorption spectra (300–500 nm) of wsCDs treated with  $\text{H}_2\text{O}$ , 100  $\mu\text{M H}_2\text{O}_2$ , and a complete peroxide system, (5  $\mu\text{g ml}^{-1}$  human origin MPO, 140 mM NaCl, and 100  $\mu\text{M H}_2\text{O}_2$ ) for 24 h; (B) UV absorbance of wsCDs suspended under various conditions at 400 nm. The results represent mean  $\pm$  SD. Statistical analysis through one-way ANOVA followed by Tukey's *post hoc* test. \*\* $p$ -value < 0.01 (treatments vs.  $\text{H}_2\text{O}$  suspension).



(Fig. 9A and B). The body's initial line of defense comprises resident macrophages and neutrophils, which generate an MPO driven peroxide system against invading pathogens and foreign materials.<sup>59</sup> For the enzymatic degradation of the CDs MPO binds to their surface OH groups present around defect sites,

and breaks down the graphitic lattice through the catalytic production of sodium hypochlorous acid (NaHOCl).<sup>20,59</sup> In the wsCDs the presence of OH was verified through the FTIR spectra (Fig. 2B). In the environment, biodegradation of organic materials is performed by a similar MPO-like bacterial peroxidases

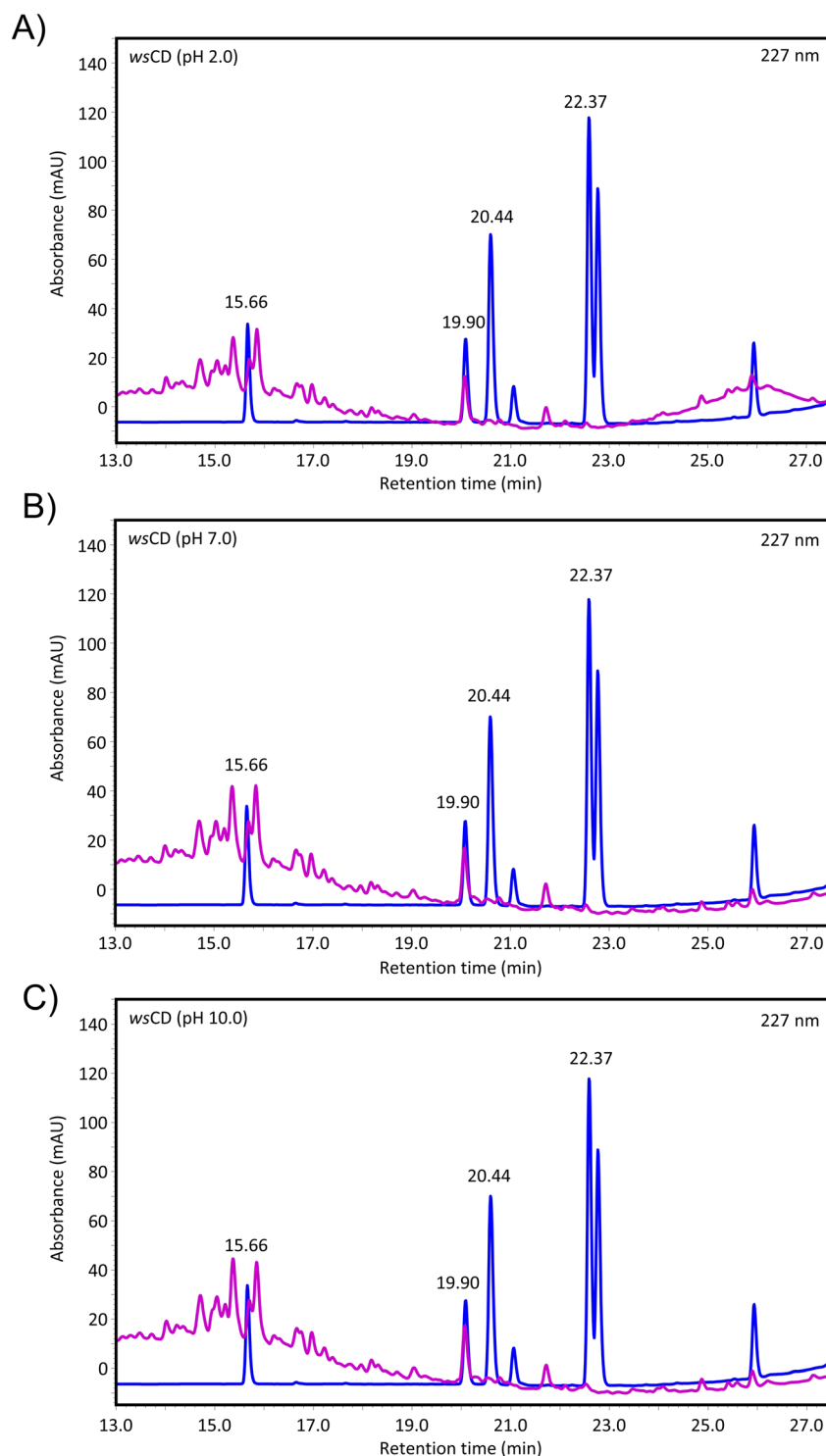


Fig. 10 pH stability of phytochemicals loaded onto wsCDs. The phytochemical content of wsCDs was analyzed using high-performance liquid chromatography (withanoside IV (15.66 min); withanoside IV (19.90 min); withaferine A (20.44 min); and withanolide A (22.37 min)) following treatments at (A) pH 2.0, (B) pH 7.0, and (C) 10.0. Quantitative data are presented in Table 2. The complete spectral range is provided in ESI image 2.†



Table 2 pH stability of phytochemicals present in wsCDs (representative HPLC spectra are presented in Fig. 10A–C)

S. No.	Marker compounds	wsCD pH 2.0 ( $\mu\text{g mg}^{-1}$ )	wsCD pH 7.0 ( $\mu\text{g mg}^{-1}$ )	wsCD pH 10.0 ( $\mu\text{g mg}^{-1}$ )
1	Withanoside IV	1.706	1.998	1.850
2	Withanoside V	1.080	1.168	1.115
3	Withanolide A	0.035	0.047	0.049
<b>Total withanolides</b>		<b>2.7895</b>	<b>3.213</b>	<b>3.041</b>

system.<sup>60,61</sup> wsCDs also function as nanovectors delivering phytochemicals loaded onto them into cell-based systems.

These phytochemicals are exposed to a range of acidic to basic pH during the uptake and biodegradation of the wsCDs. Therefore, the pH stability of the phytochemicals present in wsCDs was checked by suspending wsCDs under pH different conditions (2.0, 7.0, and 10.0) for 24 h. Using an HPLC instrument the total withanolide content was observed at  $2.79 \mu\text{g ml}^{-1}$  at pH 2.0,  $3.21 \mu\text{g ml}^{-1}$  at pH 7.0, and  $3.04 \mu\text{g ml}^{-1}$  at pH 10.0 indicating a minor reduction in phytochemical load under acidic pH conditions (Fig. 10A–C; Table 2 and ESI Fig. S2†). Taken together, the wsCDs demonstrated strong UV absorption and PL, along with great biocompatibility, antioxidant activity, and wound healing qualities under *in vitro* conditions in epidermal A431 cells. Future research work will determine the protective effect of wsCDs in eliminating DNA adduct formations induced by UVB and their own genomic interaction compared to the other commercially available nanoparticles used in cosmeceuticals and sunscreens.

## 4. Conclusion

The wsCDs displayed excellent sun protection qualities through absorption in the UV regions of 280–400 nm and photoluminescence while they carried the essential withanolides originating from the *Withania somnifera* (L.) Dunal extract. The human epidermal A431 cells were shielded by wsCDs from oxidative stress and cell viability loss brought on by UVB exposure. They accelerated wound healing by increasing the expression of growth factor mRNA in A431 cells. Under acidic pH circumstances, wsCDs were discovered to be enzymatically biodegradable with a little change in their phytochemical contents. Thus, the results support the benefits of wsCDs as a nanocosmeceutical for therapeutic applications and a sun-protection nanocomponent.

## Author contributions

AB, KB and AV contributed to the conceptualization of the study; KB and MT developed methodology and performed experimental work under the supervision of AB and AV; KB wrote the original draft and AB, MT and AV reviewed and performed the editing of the manuscript.

## Conflicts of interest

Acharya Balkrishna is a trustee in the Divya Yog Mandir Trust, Haridwar, India that governs Divya Pharmacy, Haridwar. In

addition, Acharya Balkrishna is one of the founding promoters and holds an honorary managerial position at Patanjali Ayurved Ltd, Haridwar, India. These organizations were not involved in any aspects of this study. All other authors, Meenu Tomar, Kunal Bhattacharya and Anurag Varshney are employed at the Patanjali Research Institute which is governed by the Patanjali Research Foundation Trust (PRFT), Haridwar, Uttarakhand, India, a not-for-profit organization. In addition, Anurag Varshney is an Adjunct Professor in the Department of Allied and Applied Sciences, University of Patanjali, Haridwar, India; and in the Special Centre for Systems Medicine, Jawaharlal Nehru University, New Delhi, India. All other authors declare no competing interests.

## Acknowledgements

The authors would like to acknowledge Mr Vallabh P. Mulla and Dr Jyotish Srivastava for providing the *Withania somnifera* root extract. The authors also acknowledge Mr Sudeep Verma, Dr Rohit K. Singh, and Mr Pooja Singh for their great technical assistance with HPLC analysis and biodegradation studies. We are grateful for the prompt administrative assistance provided by Mr Tarun Rajput, Mr Gagan Kumar, and Mr Lalit Mohan. The authors would like to thank the Patanjali Research Foundation Trust for funding the study.

## References

- 1 N. Kollias, E. Ruvolo Jr and R. M. Sayre, *Photochem. Photobiol.*, 2011, **87**, 1474.
- 2 R. B. Weller, *Photochem. Photobiol. Sci.*, 2017, **16**, 374.
- 3 D. Q. Andrews, K. Rauhe, C. Burns, E. Spilman, A. M. Temkin, S. Perrone-Gray, O. V. Naidenko and N. Leiba, *Photodermatol., Photoimmunol. Photomed.*, 2022, **38**, 224.
- 4 USFDA, *OTC Monograph M020*, 2021.
- 5 K. Bhattacharya, G. Kilic, P. M. Costa and B. Fadeel, *Nanotoxicology*, 2017, **11**, 809.
- 6 K. Bhattacharya, M. Davoren, J. Boertz, R. P. Schins, E. Hoffmann and E. Dopp, *Part. Fibre Toxicol.*, 2009, **6**, 17.
- 7 C. C. Lee, Y. H. Lin, W. C. Hou, M. H. Li and J. W. Chang, *Int. J. Environ. Res. Public Health*, 2020, **17**, 1.
- 8 S. Yuan, J. Huang, X. Jiang, Y. Huang, X. Zhu and Z. Cai, *Nanomaterials*, 2022, **12**, 699.
- 9 S. W. Chen, W. H. Lv, K. Wu, G. H. Chen, F. Chen, C. C. Song and Z. Luo, *Int. J. Mol. Sci.*, 2021, **22**, 12047.



- 10 A. P. Gondikas, F. v. d. Kammer, R. B. Reed, S. Wagner, J. F. Ranville and T. Hofmann, *Environ. Sci. Technol.*, 2014, **48**, 5415.
- 11 R. Cunha and L. de Brito-Gitirana, *Ecotoxicol. Environ. Saf.*, 2020, **203**, 111032.
- 12 Y. Li, Y. He, C. H. Lam and T. Nah, *Sci. Total Environ.*, 2022, **839**, 156145.
- 13 I. B. Miller, M. Moeller, M. Y. Kellermann, S. Nietzer, V. Di Mauro, E. Kamyab, S. Pawlowski, M. Petersen-Thiery and P. J. Schupp, *Toxics*, 2022, **10**, 244.
- 14 J. de Oliveira-Lima, R. L. Dias da Cunha and L. de Brito-Gitirana, *J. Environ. Sci. Health, Part B*, 2022, **57**, 81.
- 15 S. Suh, C. Pham, J. Smith and N. A. Mesinkovska, *Int. J. Dermatol.*, 2020, **59**, 1033.
- 16 L. Etordevic, F. Arcudi, M. Cacioppo and M. Prato, *Nat. Nanotechnol.*, 2022, **17**, 112.
- 17 A. Sciortino, A. Cannizzo and F. Messina, *C*, 2018, **4**, 67.
- 18 G. Hu, B. Lei, X. Jiao, S. Wu, X. Zhang, J. Zhuang, X. Liu, C. Hu and Y. Liu, *Opt. Express*, 2019, **27**, 7629.
- 19 Q. Zeng, D. Shao, X. He, Z. Ren, W. Ji, C. Shan, S. Qu, J. Li, L. Chen and Q. Li, *J. Mater. Chem. B*, 2016, **4**, 5119.
- 20 C. Martin, G. Jun, R. Schurhammer, G. Reina, P. Chen, A. Bianco and C. Menard-Moyon, *Small*, 2019, **15**, e1905405.
- 21 H. B. Shilpashree, S. J. Sudharshan, A. K. Shasany and D. A. Nagegowda, *Sci. Rep.*, 2022, **12**, 1602.
- 22 A. Balkrishna, S. Verma, V. P. Mulay, A. K. Gupta, S. Haldar and A. Varshney, *PLoS Neglected Trop. Dis.*, 2022, **16**, e0010484.
- 23 A. Balkrishna, S. K. Solleti, H. Singh, N. Sharma and A. Varshney, *Planta Med.*, 2022, **88**, 466.
- 24 M. H. Mirjalili, E. Moyano, M. Bonfill, R. M. Cusido and J. Palazon, *Molecules*, 2009, **14**, 2373.
- 25 C. A. Schneider, W. S. Rasband and K. W. Eliceiri, *Nat. Methods*, 2012, **9**, 671.
- 26 A. Suarez-Arnedo, F. Torres Figueroa, C. Clavijo, P. Arbelaez, J. C. Cruz and C. Munoz-Camargo, *PLoS One*, 2020, **15**, e0232565.
- 27 S. P. Mukherjee, A. R. Gliga, B. Lazzaretto, B. Brandner, M. Fielden, C. Vogt, L. Newman, A. F. Rodrigues, W. Shao, P. M. Fournier, M. S. Toprak, A. Star, K. Kostarelos, K. Bhattacharya and B. Fadeel, *Nanoscale*, 2018, **10**, 1180.
- 28 S. Qu, X. Wang, Q. Lu, X. Liu and L. Wang, *Angew. Chem., Int. Ed. Engl.*, 2012, **51**, 12215.
- 29 R. Duval and C. Duplais, *Nat. Prod. Rep.*, 2017, **34**, 329.
- 30 V. N. Mochalin and Y. Gogotsi, *J. Am. Chem. Soc.*, 2009, **131**, 4594.
- 31 N. Murugan and A. K. Sundramoorthy, *New J. Chem.*, 2018, **42**, 13297.
- 32 M. Tan, L. Zhang, R. Tang, X. Song, Y. Li, H. Wu, Y. Wang, G. Lv, W. Liu and X. Ma, *Talanta*, 2013, **115**, 950.
- 33 N. K. Khairol Anuar, H. L. Tan, Y. P. Lim, M. S. So'uib and N. F. Abu Bakar, *Front. Energy Res.*, 2021, **9**, 626549.
- 34 G. Gedda, C.-Y. Lee, Y.-C. Lin and H.-f. Wu, *Sens. Actuators, B*, 2016, **224**, 396.
- 35 V. N. Mehta, S. Jha, H. Basu, R. K. Singhal and S. K. Kailasa, *Sens. Actuators, B*, 2015, **213**, 434.
- 36 C. Wang, H. Shi, M. Yang, Y. Yan, E. Liu, Z. Ji and J. Fan, *Mater. Res. Bull.*, 2020, **124**, 110730.
- 37 J. Joseph and A. A. Anappara, *J. Lumin.*, 2017, **192**, 761.
- 38 C. Wang, K. Jiang, Q. Wu, J. Wu and C. Zhang, *Chemistry*, 2016, 14475, DOI: [10.1002/chem.201602795](https://doi.org/10.1002/chem.201602795).
- 39 L. Guo, J. Ge, W. Liu, G. Niu, Q. Jia, H. Wang and P. Wang, *Nanoscale*, 2016, **8**, 729.
- 40 C. Das, H. B. Samal, V. K. Meher, A. Mohanty and S. Dash, *Ann. Phytomed.*, 2022, **11**, 493–504.
- 41 F. Mirzajani, A. Ghassempour, M. Jalali-Heravi and M. H. Mirjalili, *Phytochem. Anal.*, 2010, **21**, 544.
- 42 I. A. Zlatkiy, A. V. Zlatska, N. V. Antipova, S. A. Dolenko, I. M. Gordiienko, O. S. Gubar, R. G. Vasyliiev, D. A. Zubov, S. N. Novikova and A. V. Syroeshkin, *Sci. World J.*, 2020, **2020**, 2373021.
- 43 T. G. Chatzimitakos, A. Kasouni, A. Troganis, I. Leonardos, I. Tzovenis, A. Ntzouvaras and C. Stalikas, *C-J. Carbon Res.*, 2020, **6**, 69.
- 44 S. C. Hess, F. A. Permatasari, H. Fukazawa, E. M. Schneider, R. Balgis, T. Ogi, K. Okuyama and W. J. Stark, *J. Mater. Chem. A*, 2017, **5**, 5187.
- 45 X. Feng, Y. Zhao, Y. Jiang, M. Miao, S. Cao and J. Fang, *Carbohydr. Polym.*, 2017, **161**, 253.
- 46 D. Zuo, N. Liang, J. Xu, D. Chen and H. Zhang, *Cellulose*, 2019, **26**, 4205.
- 47 D. E. Heck, A. M. Vetrano, T. M. Mariano and J. D. Laskin, *J. Biol. Chem.*, 2003, **278**, 22432.
- 48 K. Senthil, P. Thirugnanasambantham, T. J. Oh, S. H. Kim and H. K. Choi, *PLoS One*, 2015, **10**, e0123360.
- 49 S. T. Devkar, S. D. Jagtap, S. S. Katyare and M. V. Hegde, *J. Planar Chromatogr.–Mod. TLC*, 2014, **27**, 157.
- 50 S. Mathur, P. Kaur, M. Sharma, A. Katyal, B. Singh, M. Tiwari and R. Chandra, *Phytomedicine*, 2004, **11**, 452.
- 51 J. W. Penn, A. O. Grobbelaar and K. J. Rolfe, *Int. J. Burns Trauma*, 2012, **2**, 18.
- 52 J. Hardwicke, D. Schmaljohann, D. Boyce and D. Thomas, *Surgeon*, 2008, **6**, 172.
- 53 T. Quan, T. He, S. Kang, J. J. Voorhees and G. J. Fisher, *J. Invest. Dermatol.*, 2002, **119**, 499.
- 54 M. Seo, M.-J. Lee, J. H. Heo, Y.-I. Lee, Y. Kim, S.-Y. Kim, E.-S. Lee and Y.-S. Juhnn, *J. Biol. Chem.*, 2007, **282**, 24720.
- 55 H. Wang and I. E. Kochevar, *Free Radical Biol. Med.*, 2005, **38**, 890.
- 56 I. Pastar, O. Stojadinovic, A. Krzyzanowska, S. Barrientos, C. Stuelten, K. Zimmerman, M. Blumenberg, H. Brem and M. Tomic-Canic, *Mol. Med.*, 2010, **16**, 92.
- 57 A. Sikandan, T. Shinomiya and Y. Nagahara, *Int. J. Mol. Med.*, 2018, **42**, 425.
- 58 K. Bhattacharya, S. P. Mukherjee, A. Gallud, S. C. Burkert, S. Bistarelli, S. Bellucci, M. Bottini, A. Star and B. Fadeel, *Nanomedicine*, 2016, **12**, 333.
- 59 V. E. Kagan, N. V. Konduru, W. Feng, B. L. Allen, J. Conroy, Y. Volkov, I. I. Vlasova, N. A. Belikova, N. Yanamala, A. Kapralov, Y. Y. Tyurina, J. Shi, E. R. Kisin, A. R. Murray, J. Franks, D. Stolz, P. Gou, J. Klein-Seetharaman, B. Fadeel, A. Star and A. A. Shvedova, *Nat. Nanotechnol.*, 2010, **5**, 354.
- 60 N. Bansal and S. S. Kanwar, *Sci. World J.*, 2013, **2013**, 714639.
- 61 L. Zhang, E. J. Petersen, M. Y. Habteselassie, L. Mao and Q. Huang, *Environ. Pollut.*, 2013, **181**, 335.

